Transmission Electron Microscopy Studies of Ge Nanocrystals

Q. Xu[a,b], I.D. Sharp[a,b], C.Y. Liao[a,b], D. O. Yi[a,c], J.W. Ager III[a], J.W. Beeman[a], Z. Liliental-Weber[a], K.M. Yu[a], D. Zakharov[a], D. C. Chrzan[a,b], E.E. Haller[a,b]
[a]Materials Sciences Division, Lawrence Berkeley National Laboratory, Berkeley, CA 94720, USA
[b]Department of Materials Science and Engineering, University of California, Berkeley, CA 94720, USA
[c]Applied Science and Technology Group, University of California, Berkeley, CA 94720, USA

ABSTRACT

Electron microscopy studies of ^{74}Ge and ^{70}Ge nanocrystals formed by ion beam synthesis in SiO_2 are presented. Cross-sectional transmission electron microscopy (TEM) is used to determine the crystallinity and the size distribution. The observation of numerous twinned nanocrystals is consistent with process-induced compressive stress, which was also found by Raman spectroscopy. The nanocrystals are released from the SiO_2 matrix by etching in a HF bath and examined in a Philips CM200 TEM. High-resolution micrographs and selective area diffraction confirm that the crystallinity is retained in this process and also show an amorphous shell encapsulating the released nanocrystals. Transfer of released nanocrystals is achieved through ultrasonic dispersion in methanol and deposition onto lacey carbon films via evaporation of methanol. In an effort to determine the melting point of Ge nanocrystals and observe the growth and evolution of nanocrystals embedded in the amorphous SiO_2 during heat treatment, as-grown nanocrystals were heated *in-situ* up to 1192˚C ± 60˚C in a JEOL 200CX analytical electron microscope. Electron diffraction patterns are recorded using a Charge-Coupled Device. A large melting hysteresis was observed around the melting temperature of bulk Ge.

INTRODUCTION

Embedded Ge nanocrystals have attracted strong interest worldwide due to promising non-volatile memory applications [1-3] and quantum mechanical predictions of efficient size-dependent photoluminescence [4]. Among various methods of embedded nanocrystal fabrication, ion beam synthesis has the advantages of compatibility with existing microfabrication processes and precise control of isotopes and spatial distribution.

Ion-beam synthesized nanocrystals can exhibit a large compressive stress after post implantation annealing [5-6]. The stress state of these nanocrystals can be controlled by post-growth thermal treatments so as to finely tune the energy band structure [7]. However the origin of this stress is still unclear. It is known that Ge has a 5% volume increase upon solidification; therefore it is vital to determine the state of these nanocrystals at growth temperature. Freestanding nanocrystals have been reported to have a reduced melting point compared to bulk material due to the large surface area to volume ratio [8-10]. In contrast,

observations of embedded nanocrystals have shown hysteresis behavior around the bulk melting temperature [11]. The fundamental thermal properties are influenced by the surface phonon modes of the nanocrystals, thus it is very important to obtain a better understanding of the growth process at annealing temperature.

EXPERIMENT

500 nm silicon dioxide thin films were grown by wet oxidation of (100) oriented Si substrates. Isotopically pure ^{70}Ge or ^{74}Ge nanocrystals were fabricated via selective ion implantation. In order to achieve a more uniform distribution of concentration, a multi-energy/dose implantation scheme was chosen: 50 keV (1×10^{16} cm^{-2}), 80 keV (1.2×10^{16} cm^{-2}), and 120 keV (2×10^{16} cm^{-2}) [12]. Following implantation, samples were annealed in an Ar atmosphere for 60 min at 900˚C, and were subsequently quenched from the annealing temperature to room temperature under running water. Cross-sectional and plan-view TEM studies were performed to obtain structure information and size distributions.

Nanocrystals were liberated from the matrix via selective hydrofluoric acid (HF) etching of the oxide film using 1:1 49% HF:H_2O solution. Exposed nanocrystals were then transferred to a lacey carbon film grid via ultrasonic dispersion in methanol. This transfer was performed in two steps. First, the as-etched samples were placed into a methanol bath and sonicated for 60 minutes. Second, the lacey carbon grid was immediately immersed into the just dispersed nanocrystal-containing methanol solution while the methanol was evaporated away in a constant nitrogen gas stream. Powder electron diffraction patterns were obtained in JEOL 200CX analytical electron microscope at 200kV indicating crystalline Ge nanoclusters.

A selectively etched plan-view TEM specimen was prepared by adding a HF etching step between backside dimpling and backside ion-milling. This specimen was then characterized in a Philips CM200 TEM. High resolution TEM (HR-TEM) micrographs were obtained.

As-grown nanocrystal samples were heated in-situ up to 1192˚C ± 60˚C in a JEOL 200CX analytical electron microscope operating at 200 kV. The heating and cooling runs were conducted in 15-50˚C/min steps using a Gatan 628Ta single tilt heating holder. Three cycles of heating-cooling were repeated for the same specimen. Electron diffraction patterns were recorded *in-situ* onto videotape through a Charge-Coupled Device. The beam current was kept at 8 μA above dark current so as to minimize beam heating [9].

RESULTS

Shown in Fig. 1 are the cross-sectional TEM micrographs of the as-grown ^{74}Ge nanocrystals and a HR-TEM micrograph of an individual nanocrystal. The nanocrystals were grown with a mean diameter of 5.1 nm with a FWHM of 3.9 nm in the near-surface region of the oxide film. Twinned and perfect spherical nanocrystals were observed. The arrow in Fig. 1b indicates the location of a twinning plane [13].

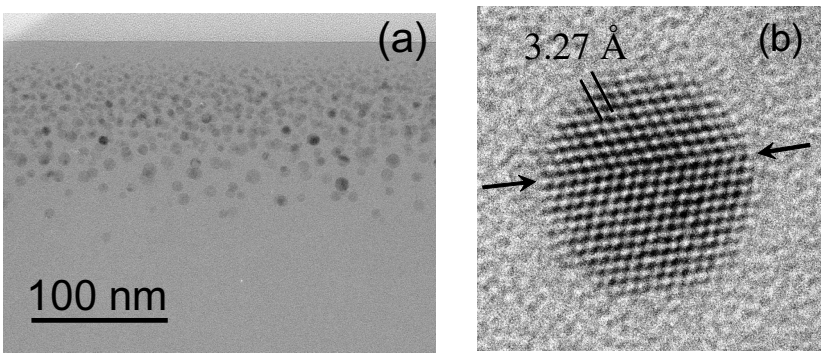

Figure 1. a) Cross-sectional TEM micrograph of ion beam synthesized ^{74}Ge nanocrystals embedded in SiO_2. b) High Resolution TEM micrograph of a 5.3 nm diameter nanocrystal with the expected lattice constant. Arrows indicate the location of a single twinning plane.

The diffraction patterns (DPs) for as-grown and transferred nanocrystals are shown in Fig. 2. The fact that the DPs were present at all times suggests that the crystallinity is retained through the etching and solution dispersion process. However, the two DPs differ from each other. Higher order rings were more discernable in selectively etch-exposed nanocrystals. Since there was no special surface passivation for the nanocrystals in the methanol ultrasonic dispersion process, agglomeration is very likely to happen. Bright field observations also showed that only a fraction of the nanocrystals were deposited onto the lacey carbon film during evaporation.

An as-etched specimen was further studied under high resolution. The micrographs in Fig. 3 show some Ge nanocrystals residing on the edge of the Si (001) substrate. The lattice spacing of the shown nanocrystals corresponds to Ge {111}. Preliminary X-ray photoelectron spectroscopy (XPS) measurements indicate the existence of Ge-O bonds in the surface 2 to 3 atomic layers. Although these nanocrystals are directly exposed to air ambient, they remain crystalline and unoxidized up to at least 5 months [13].

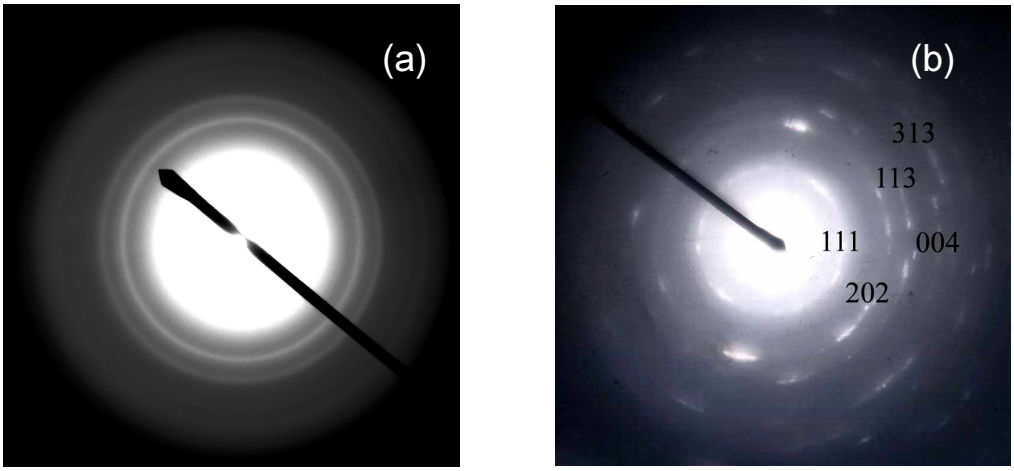

Figure 2. a) Electron diffraction pattern of ion beam synthesized ^{74}Ge nanocrystals embedded in SiO_2. b) Electron diffraction pattern of etch-exposed ^{74}Ge nanocrystals transferred on a lacey carbon grid.

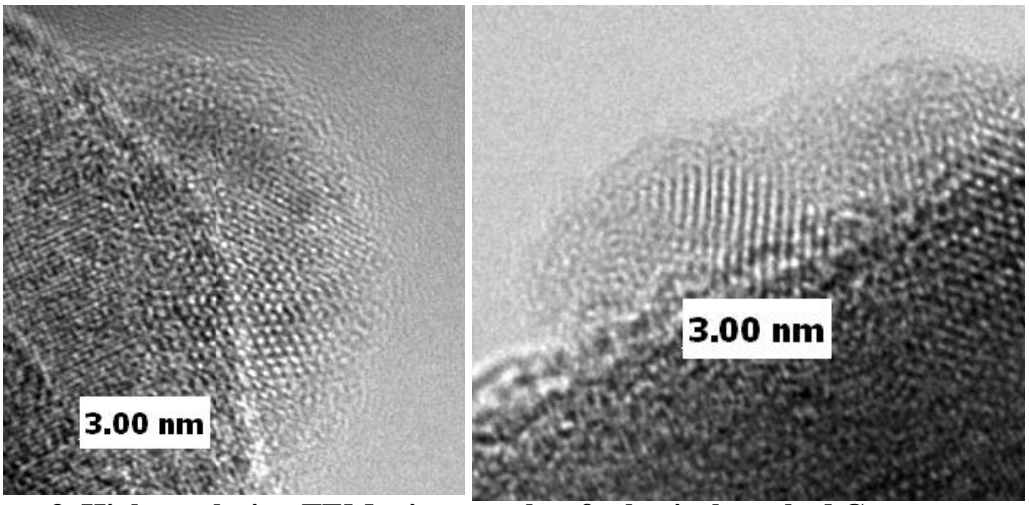

Figure 3. High resolution TEM micrographs of selectively etched Ge nanocrystals sitting on a (001) Si substrate. The as-shown nanocrystals are located on the edge of the hole.

The as-grown Ge nanocrystals exhibit a compressive stress of around 1.6GPa determined by Raman spectroscopy measurements [14]. There are several processes that can lead to this stress. The thermal expansion difference between Ge and SiO_2 matrix is too small and of the opposite sign to account for the large as-grown stress. Ge undergoes a 5% volume increase when it transforms from the liquid to the solid phase. If the Ge nanoclusters are formed in the liquid phase, a possible phase transition upon quenching would result in large compressive stresses, as are observed. The characterization of the melting behavior of embedded Ge nanocrystals was conducted using an as-grown sample. The electron diffraction pattern was videotaped in-situ as the temperature was varied. Figure 4 shows a typical captured electron DP. As the temperature was increased, the contrast of the DP decreased as expected due to the decreasing Debye-Waller factor. At higher temperatures, the diffraction pattern disappeared due to loss of crystallinity. A gradual transition of contrast change with temperature was observed. This is attributed to the size dependence of the melting temperature of the nanocrystals and the fact that the nanocrystals have a size distribution.

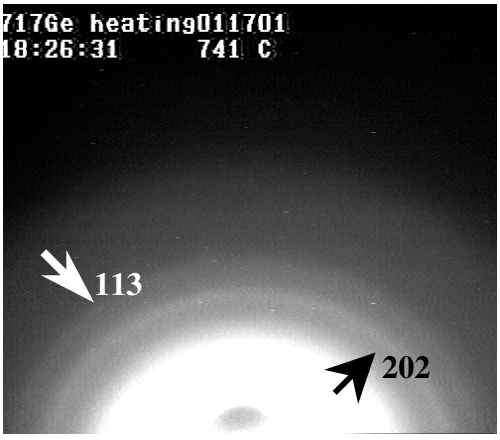

Figure 4. Electron diffraction pattern from embedded Ge nanocrystals captured at 741˚C.

The rings corresponding to {202} and {113} lattice spacing of Ge are clearly visible in Fig. 4. The first 111 peak is buried in the saturation region of the transmitted primary electron beam. The intensity profiles of the DP images at different temperatures were obtained by angular integration. The amorphous scattering background (i.e., the intensity profile at the highest temperature at which the DP of the nanocrystals totally lost contrast) has been subtracted from the profiles shown in Fig. 5. Figure 5a demonstrates the peak intensity change with temperature in the heating cycle. Figure 5b shows the peak intensity change in the

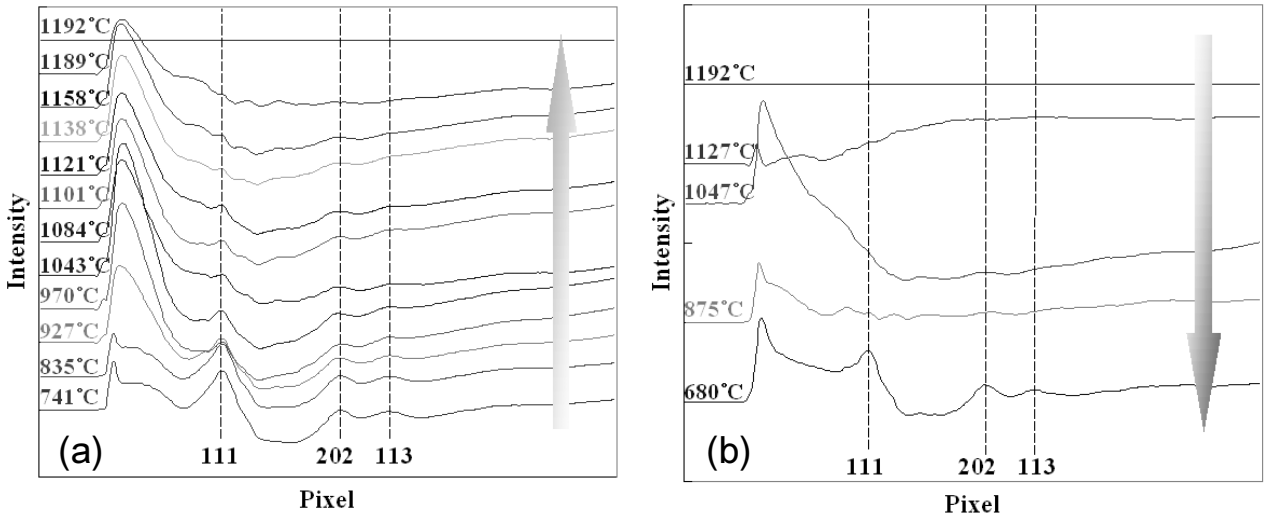

Figure 5. a) The intensity profiles of the electron diffraction pattern from embedded Ge nanocrystals as temperature increased. b) The intensity profiles of the electron diffraction pattern from embedded Ge nanocrystals as temperature decreased.

cooling cycle. The ring corresponding to {111} lattice spacing has prominent intensity after background subtraction. During the heating cycle, the intensities of all the three low index rings decreased as temperature increased. This is consistent with the temperature dependence of the Debye-Waller factor. However, all three rings are observable up to 1121˚C. This indicates a significant superheating above the melting point of bulk Ge 937˚C. Figure 5b shows an undercooling of the same magnitude in the cooling cycle. The low index peaks only reappear at 680˚C. We believe this 400˚C melting hysteresis arises from the interface property of the nanocrystals. More heating-cooling cycles were performed on the same sample. Similar hysteresis was observed but with a reduced magnitude. The reduction of the hysteresis can be expected based on coarsening of these nanocrystals during the thermal cycles.

CONCLUSIONS

Isotopically controlled Ge nanocrystals were synthesized by selective ion implantation into a SiO_2 matrix. Liberation and transfer of these nanocrystals without loss of crystallinity were successful as indicated by TEM results. The exposed nanocrystals have an amorphous shell and remain stable in ambient air. In-situ TEM heating experiments showed that the embedded Ge nanocrystals exhibit a large melting hysteresis around the melting point of bulk Ge. The thermal properties of nanocrystals can be significantly influenced by the surface atoms vibrations.

ACKNOWLEDGMENTS

D.C.C. and E.E.H. acknowledge support by the Miller Institute for Basic Research in Science. This work was supported in part by US NSF Grant Nos. DMR-0109844 and EEC-0085569, and by the Director, Office of Science, Office of Basic Energy Sciences, Division

of Materials Sciences and Engineering, of the U.S. Department of Energy under Contract No. DE-AC03-76SF00098.

REFERENCES

1. S. Tiwari, F. Rana, H. Hanafi, A. Hartstein, E. F. Crabbe, and K. Chan, Appl. Phys. Lett. **68**, 1377 (1996).
2. L. Rebohle, J. von Borany, H. Fröb, and W. Skorupa, Appl. Phys. B **71**, 131 (2000).
3. J. von Borany, T. Gebel, K. -H. Stegemann, H. -J. Thees, and M. Wittmaack, Solid-State Electron. **46**, 1729 (2002).
4. T. Takagahara and K. Takeda, Phys. Rev. B **46**, 578 (1992).
5. A. Wellner, V. Paillard, C. Bonafos, H. Coffin, A. Claverie, B. Schmidt and K. H. Heinig, J. Appl. Phys. **94**, 5639 (2003).
6. M. Dubiel, S. Brunsch, W. Seifert, H. Hofmeister, and G.L. Tan, Eur. Phys. J. D **16**, 229 (2001).
7. S. Wei and A. Zunger, Phys. Rev. B **60**, 5404 (1999).
8. M. Takagi, J. Phys. Soc. Jpn. **9,** 359 (1954).
9. A. N. Goldstein, C. M. Echer, and A. P. Alivisatos, Science **256** (5062), 1425 (1992).
10. Y. Wu and P. Yang, Appl. Phys. Lett. **77**, 43 (2000)
11. H. Andersen and E. Johnson, Nucl. Instrum. Methods B **106**, 480 (1995).
12. M. Yamamoto, T. Kashikawa, T. Yasue, H. Harima, and K. Kajiyama, Thin Solid Films **369**, 100 (2000).
13. I. D. Sharp, Q. Xu, C. Y. Liao, J.W. Ager III, J. W. Beeman, K. M. Yu, D. Zakharov, Z. Liliental-Weber, and E. E. Haller, Mater. Res. Soc. Symp. Proc. **777**, T7.6 (2003).
14. D. O. Yi, I. D. Sharp, Q. Xu, C. Y. Liao, J. W. Ager, J. W. Beeman, Z. Liliental-Weber, K. M. Yu, D. Zakharov, E. E. Haller, and D. C. Chrzan, MRS Spring Meeting, Symposium P (2004).